

Article

Functionalization of a Hydrophilic Commercial Membrane Using Inorganic-Organic Polymers Coatings for Membrane Distillation

Lies Eykens ^{1,2,*}, Klaus Rose ³, Marjorie Dubreuil ¹, Kristien De Sitter ¹, Chris Dotremont ¹, Luc Pinoy ⁴ and Bart Van der Bruggen ^{2,5}

¹ VITO-Flemish Institute for Technological Research, Boeretang 200, 2400 Mol, Belgium; marjorie.dubreuil@vito.be (M.D.); kristien.desitter@vito.be (K.D.S.); chris.dotremont@vito.be (C.D.)

² Department of Chemical Engineering, KU Leuven, Celestijnenlaan 200F, B-3001 Leuven, Belgium; bart.vanderbruggen@kuleuven.be

³ Fraunhofer Institute for Silicate Research ISC, Neunerplatz 2, 97082 Würzburg, Germany; Klaus.rose@isc.fraunhofer.de

⁴ Department of Chemical Engineering, Cluster Sustainable Chemical Process Technology, KU Leuven, Gebroeders Desmetstraat 1, B-9000 Ghent, Belgium; luc.pinoy@kuleuven.be

⁵ Faculty of Engineering and the Built Environment, Tshwane University of Technology, Private Bag X680, Pretoria 0001, South Africa

* Correspondence: lies.eykens@vito.be; Tel.: +32-14-335-663

Academic Editor: Faisal Hai

Received: 3 May 2017; Accepted: 16 June 2017; Published: 20 June 2017

Abstract: Membrane distillation is a thermal separation technique using a microporous hydrophobic membrane. One of the concerns with respect to the industrialization of the technique is the development of novel membranes. In this paper, a commercially available hydrophilic polyethersulfone membrane with a suitable structure for membrane distillation was modified using available hydrophobic coatings using ORMOCER[®] technology to obtain a hydrophobic membrane that can be applied in membrane distillation. The surface modification was performed using a selection of different components, concentrations, and application methods. The resulting membranes can have two hydrophobic surfaces or a hydrophobic and hydrophilic surface depending on the application method. An extensive characterization procedure confirmed the suitability of the coating technique and the obtained membranes for membrane distillation. The surface contact angle of water could be increased from 27° up to 110°, and fluxes comparable to membranes commonly used for membrane distillation were achieved under similar process conditions. A 100 h test demonstrated the stability of the coating and the importance of using sufficiently stable base membranes.

Keywords: hydrophobic coatings; direct contact membrane distillation (DCMD); polyethersulfone; ORMOCER[®]; wetting

1. Introduction

Membrane distillation (MD) is a thermal separation technique using a hydrophobic microporous membrane as a contactor between two liquid phases. The membrane allows vapors (e.g., water vapor) to permeate, whereas the liquid phase including the dissolved components (e.g., salts) is retained by the membrane. A temperature difference induces the driving force and allows vapors to permeate from the hot feed side to the cold permeate side. The technique was initially proposed as an alternative technology for reverse osmosis in seawater desalination. However, due to the benefits of very high retentions and less dependence on salinity, it is recently also proposed for applications beyond the scope of reverse osmosis. The applications can include but are not limited to desalination and brine

treatment [1], waste water treatment [2,3], and resource recovery [4], where the dissolved components can be salts, proteins [5], acids [2,6], and minerals [4].

Currently, hydrophobic microfiltration membranes are used in membrane distillation, although these membranes are not optimized for the MD process [7,8]. The specific requirements for membrane distillation membranes are described in literature [9–11]. Most importantly, the membrane must consist of at least one layer that is not wetted by the liquid stream under the operational pressures used in the module. The minimum pressure required to wet a hydrophobic membrane is the liquid entry pressure (*LEP*), which depends on the membrane characteristics as well as on the feed composition and is defined by the following equation:

$$LEP = \frac{-2B\gamma_l \cos(\theta)}{r_{max}} \quad (1)$$

where γ_l is the surface tension ($\text{N}\cdot\text{m}^{-1}$) of the liquid, θ the contact angle ($^\circ$), r_{max} the maximum pore size (μm), and B is a geometric factor. To ensure proper operation under fluctuating pressures and temperatures, an *LEP* of 2.5 bar is required [12]. To achieve a sufficient *LEP*, membranes with maximum pore diameter between 0.1 and 1 μm with a water contact angle above 90° are recommended for membrane distillation [9,13,14]. Moreover, it is generally agreed that a high membrane porosity is one of the most important membrane parameters in membrane distillation for both flux and energy efficiency, regardless of the MD configuration [15–19]. Additionally, membranes with a thickness between 30 up to 60 μm are recommended; however, it was shown recently that this optimal value depends on salinity, and at high salinity, thicker membranes are preferred [20]. Currently, most commercial systems use membranes not specifically developed for membrane distillation (i.e., hydrophobic polyethylene (PE), polyvinylidene fluoride (PVDF) and polytetrafluoroethylene (PTFE) microfiltration membranes). However, in the literature, many efforts are described to improve the membrane performance. These efforts include the optimization of the phase inversion process, mainly using the hydrophobic polyvinylidene fluoride (PVDF) or poly (vinylidene fluoride-co-hexafluoropropylene) (PVDF-HFP) as polymer [21–24] and the use of surface modifying macromolecules [25–27] and electrospinning [28,29]. In addition to the optimization of the membrane structure, research is also oriented toward the enhancement of the surface properties for membrane distillation, including but not limited to plasma treatment [30,31], fluorination of a TiO_2 coating [32], or the use of fluoroalkylsilane coatings on Tunisian Clay membranes [33]. Currently, these coatings are only applied in lab scale experiments and are not yet commercially available. In this publication, the use of hydrophobic sol-gel coatings forming an organic-inorganic network on hydrophilic polyethersulfone (PES) membranes is presented. These types of coatings are already used on a commercial scale, showing excellent stability in other applications, including scratch- and abrasion-resistant coatings for plastics [34], functional coatings on glass [35], and gas-sensitive layers [36]. Because of its easy scalable production method, excellent stability, and ability to functionalize the surface properties, this coating material was selected to be applied on a commercially available hydrophilic membrane with the required structure for membrane distillation [14]. The inorganic network is formed by Si-O-Si bonds, whereas the organic network is formed by reactive and polymerizable organic functional groups. The choice of hydrophobic fluorosilanes results in a surface with a hydrophobic character, whereas the unique formation of an organic-inorganic network results in a scratch- and leach-resistant coating. For the first time, these readily available coatings are applied for tuning the hydrophobicity of a cheap hydrophilic membrane to enable application in membrane distillation.

2. Materials and Methods

2.1. Membranes

The commercial hydrophilic microfiltration membrane used as base material in this study is the MicroPES[®] 2F (3M, Wuppertal, Germany). PVDF GVHP (Merck Chemicals N.V., Overijse, Belgium) is

a hydrophobic membrane commonly used in the membrane distillation literature as a reference for comparison of the performance of newly synthesized membrane distillation membranes [37–39]. PE (Solupor, Lydall, Manchester, CT, USA) is also added as a reference membrane, because it is used in commercially available membrane distillation modules.

2.2. Coatings

The commercially available and patented ORMOCER® technology was used to apply a hydrophobic coating on the MicroPES membrane. Three different combinations of silanes were explored. The three different fluorosilanes investigated in this study have a different structure, different chain length, and different hydrophobizing properties. The monomers exhibit a bifunctional character and are able to form a stable combined inorganic-organic network. The synthesis procedure is presented in Figure 1.

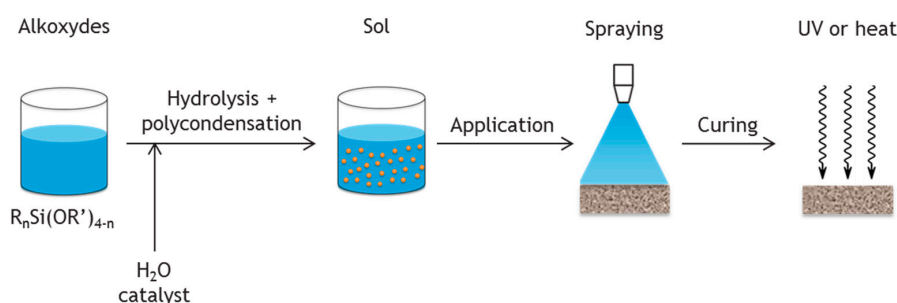


Figure 1. Coating procedure.

The process starts from an alcoholic solution of the $R'Si(OR)_3$ monomers, where R' is a functional non-reactive hydrophobic group or a polymerizable group, e.g., acryl or vinyl. R represents simple aliphatic groups, e.g., methyl or ethyl. By the addition of water and catalyst, both hydrolysis and polycondensation reactions can occur, resulting in the formation of Si-O-Si covalent bonds forming the inorganic network (Figure 2). The hydrolysis reaction results in the cleavage of a chemical bond by the addition of water. During the polycondensation reactions, two molecules combine to form a larger molecule by splitting a small molecule. Two of the OH groups formed after hydrolysis on the silica components can form H_2O (polycondensation 1), or the unreacted OR group can react with an OH group to form ROH (polycondensation 2). After multiple polycondensation steps, an inorganic polymer network with a Si-O backbone is formed, resulting in a disperse solution, called the sol.

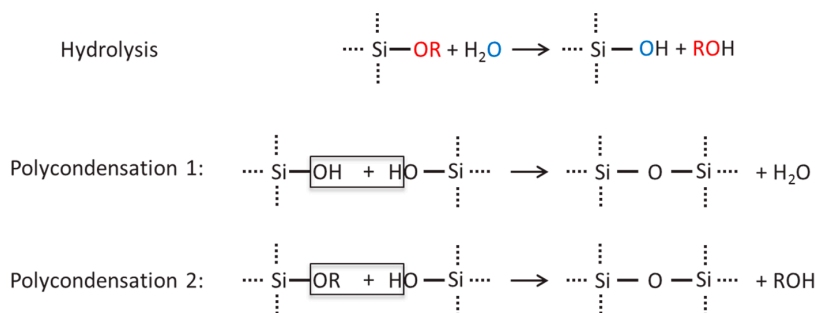


Figure 2. Mechanism of the hydrolysis and polycondensation reactions.

In a second step, this sol is applied on the membrane surface using a bar coater, a roll-to-roll system, or spray coating. Finally, the coating is cured using a thermal or photochemical curing step using ultraviolet (UV) light, in which the polymerizable groups present in the solution will form the

organic network. The nature of the chemicals used (acryl, vinyl, etc.) determines the organic network type. More details on the system can be found in the literature [34,40].

Figure 3 shows the structure of the perfluorodecyl (PFD) silane. After the sol-gel processing this single component only forms the silica network in an alcoholic solution. No polymerizable group is present in this solution and hence, no organic network is formed in this system. The PFD system was only thermally dried at 80 °C for 30 min. i.e., thermal based evaporation of the solvents (water/alcohol), which led to a solid film.

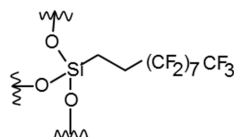
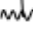


Figure 3. Single component system with perfluorodecyl (PFD),  represents the inorganic network.

The second system is a four-component system where a mono-acrylic (Ak) component forms the reactive site for acrylic polymerization. The methyl (T) and dimethyl (D) silanes as well as the highly fluorinated silane (BTFO2N) are participating as hydrophobizing component in the organic network (Figure 4). A composition of Ak/T/D/BTFO2N of 20/44/34/2 wt. % was used.

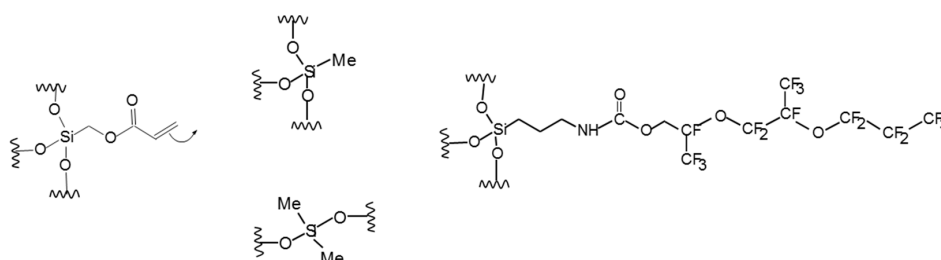




Figure 4. The second system (Ak/T/D/BTFO2N system),  represents the inorganic network,  represents the organic network formation.

The third is a three component system including a vinyl silane (V), a 3-mercaptopropyl silane (Mc) and a perfluoro-octyl silane (F13) with composition 49/49/2 wt. % V/Mc/F13 (Figure 5). The inorganic silica network is formed by the three components, while the organic network is formed by an addition reaction of the thiol-group to the vinyl group [41]. The hydrophobicity is provided by the perfluoro-octyl group. The UV-curing for the systems Ak/T/D/BTFO2N and V/Mc/F13 was performed using a mercury UV lamp, running with 1200 Watt power, a UV dose of 5000 mJ/m², and a UV curing duration 20 s. The UV-curing temperature is ca. 60–80 °C, which evolves from the UV-lamps.

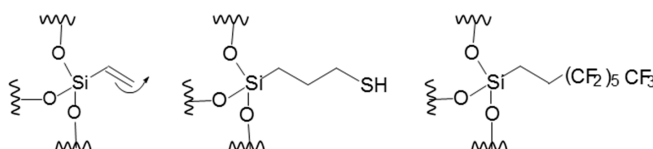


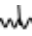

Figure 5. The third system (V/Mc/F13 system),  represents the inorganic network,  represents the organic network formation.

Table 1 shows the composition, the application method and the final network of the different coatings applied in this study. Coatings 1, 2, and 4 were applied using a roll-to-roll system, coatings 3 and 5 were applied using a bar coater system. Coatings 6 and 7 use the same components as for coating 5, but are applied using spray coating (6 as single side coating, 7 as double side coating). Coatings 1 and 2 have no reactive organic group and only differ in the mass fraction of the fluorinated

alkylsiloxane. After thermal curing, these solutions only form an inorganic network. Coatings 3 to 7 are multiple component systems and contain an organic-inorganic network. For membrane 4, a higher mass fraction of the components was used.

Table 1. Composition of the coatings used in this study (perfluorodecyl: PFD; the second system: Ak/T/D/BTFO2N; the third system: V/Mc/F13).

Coating System	Coating Components	Mass Fraction in Coating Solution	Application Method	Network Formation
1	PFD solution	5 wt. %	Roll-to-roll system	No organic crosslinking
2	PFD solution	10 wt. %	Roll-to-roll system	No organic crosslinking
3	Ak/T/D/BTFO2N	5 wt. %	Bar coater	Acrylic polymerization
4	Ak/T/D/BTFO2N	30 wt. %	Roll-to-roll system	Acrylic polymerization
5	V/Mc/F13	5 wt. %	Bar coater	Vinyl + SH addition
6	V/Mc/F13	5 wt. %	Spray coater	Vinyl + SH addition
7	V/Mc/F13	5 wt. %	Spray coater	Vinyl + SH addition

2.3. Characterization Methods

The contact angle of the membranes was measured with the OCA 15EC Contact Angle System (DataPhysics Instruments GmbH, Filderstadt, Germany) using the static sessile drop method. The liquid entry pressure was determined as described by Khayet et al. [42]. The pressure was increased slowly by 0.1 bar each 30 s, until a flow was detected. A Porolux™ 1000 device (Porometer N.V., Eke, Belgium) using the wet/dry capillary flow porometry method measured the pore size distribution as described by Francis et al. [43]. Porefil with a liquid surface tension of 16 mN·m^{−1} was used as wetting liquid and the shape factor was assumed to be 1. The porosity of the membranes was calculated using the following equation suggested by Smolders and Franken [44]:

$$\epsilon = 1 - \frac{\rho_m}{\rho_{pol}} \quad (1)$$

with ρ_m and ρ_{pol} representing the density of the membrane and the polymer, respectively, in g·cm^{−3}. The density of the membrane was obtained by measuring the mass of a circular membrane cut with a circular mold with diameter of 5 cm. The density of the polymer was measured using gas pycnometry with a He-pycnometer (Micromeritics, Norcross, GA, USA) [20]. A cold field emission scanning electron microscope (SEM) type JSM6340F (JEOL, Tokyo, Japan) was used to study membrane cross-sections at an acceleration voltage of 5 keV. Cross-sections were obtained by a cross-section polisher type SM-09010 (JEOL, Tokyo, Japan) using an argon ion beam. All samples were coated with a thin Pt/Pd layer (~1.5 nm) using a Cressington HR208 high-resolution sputter-coater (Cressington Scientific Instruments, Watford, UK) to avoid charging by the e-beam. The images of the cross-sections were analyzed in ImageJ [20].

2.4. Membrane Distillation Setup

The membrane distillation performance was evaluated with a lab-scale DCMD setup (Figure 6). The flat-sheet module had a feed and permeate channel with dimensions of 6 cm width and 18 cm length. The channel height and spacer thickness was 2 mm. On the permeate side, purified water with electrical conductivity below 20 µS·cm^{−1} was used. The feed and distillate were circulated counter-currently on their respective sides of the membrane with a flow velocity of 0.13 m/s using peristaltic pumps (Watson-Marlow, 520DuN/R2, Zwijnaarde, Belgium). $T_{f,in}$ and $T_{p,out}$ was kept constant at 60 °C and 45 °C, respectively, for all experiments. The temperatures were kept constant using two heating baths (Huber, Ministat 230w-cc-NR, Offenburg, Germany) and monitored using four thermocouples (Thermo Electric Company, PT100 TF, Balen, Belgium). The flux was measured by evaluating the weight variations in the feed and distillate tank, using an analytical balance (Sartorius GmbH, ED8801-CW, Goettingen, Germany). The average of at least two experiments

is reported. The electrical conductivity at the feed and permeate side were monitored by portable conductivity meters (WTW GmbH, pH/Cond 340i, Weilheim, Germany).

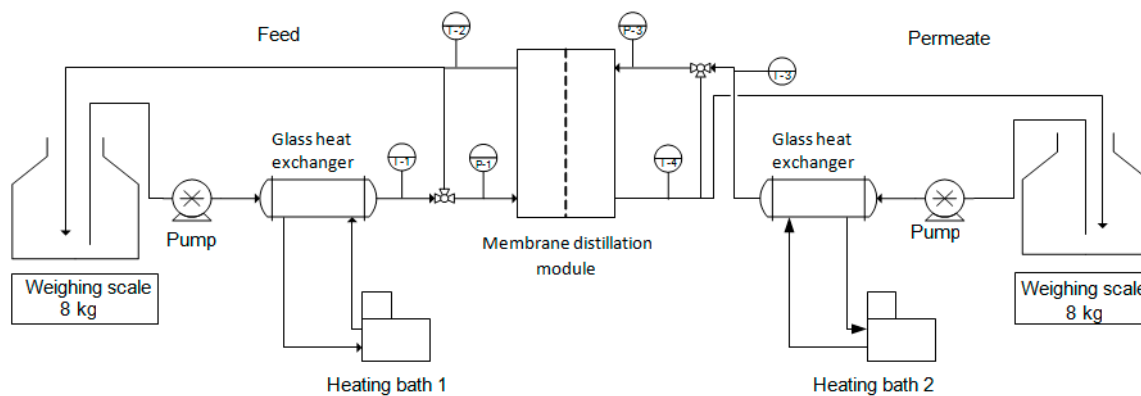


Figure 6. Schematic of the membrane distillation setup.

The energy efficiency (EE) of the process is defined in Equation (3). The total heat transfer through the membrane Q_m is considered to be equal to the heat transfer in the feed channel, as described by Khayet et al. [45].

$$EE (\%) = \frac{N \cdot \Delta H \cdot A}{F \cdot C_p \cdot (T_{in} - T_{out})} \quad (3)$$

N ($\text{kg} \cdot \text{m}^{-2} \cdot \text{h}^{-1}$) is the water flux and ΔH ($\text{J} \cdot \text{kg}^{-1}$) the enthalpy of evaporation. F is the mass flow rate in the channels expressed in $\text{kg} \cdot \text{s}^{-1}$, A (m^2) is the effective membrane surface area, C_p is the specific heat capacity of the solution ($\text{J} \cdot \text{kg}^{-1} \cdot ^\circ\text{C}^{-1}$), T_{in} and T_{out} are the bulk temperatures at the channel inlet and outlet of the module expressed in $^\circ\text{C}$, respectively. The calculations were carried out for the feed and permeate channel and the average and standard deviation are reported.

Long term stability tests were performed using $35 \text{ g} \cdot \text{L}^{-1}$ NaCl as feed concentration. The experimental conditions were chosen differently from the screening tests, because these experiments run overnight. The flux should be limited, to prevent spilling over of the permeate vessel. Therefore, lower temperatures have been chosen for these experiments: T_f and T_p were 45°C and 40°C respectively with a cross flow velocity of the feed of $0.1 \text{ m} \cdot \text{s}^{-1}$ and a salinity of $35 \text{ g} \cdot \text{L}^{-1}$. The goal of this experiment was mainly to investigate the stability of the coating under constant shear of the feed liquid, not the thermal stability. In general, the thermal stability of the hybrid coatings is 150°C and higher, up to 300°C . This thermal stability has been measured for another application elsewhere [4]. The temperature stability of the coating material is much higher compared to the temperatures generally used in MD up to 90°C and the temperature stability of this coating is not an issue for these coatings.

3. Results

3.1. Characterization of the Membranes

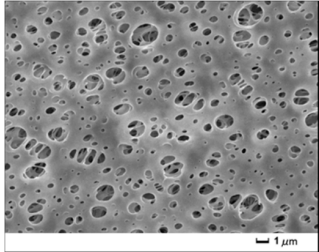
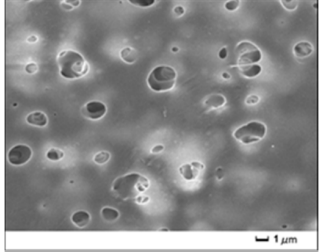
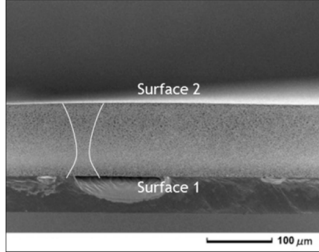
The measured properties of the MicroPES 2F membrane used as base membrane for the coatings are shown in Table 2, together with the properties of the commercial hydrophobic membranes commonly used in membrane distillation.

SEM images reveal a difference in the surface porosity on both sides of the PES-membrane (Table 3). While the pore size is larger on the surface side 2, the pore density and porosity are the highest on surface side 1. The cross-section shows an hourglass-shaped pore structure [46]. The densest zone of the membrane is located in the region of 10 to $50 \mu\text{m}$ distance from surface 1. All coatings are applied on the surface 1 because this side has the lowest pore size, which is preferred to increase the wetting resistance.

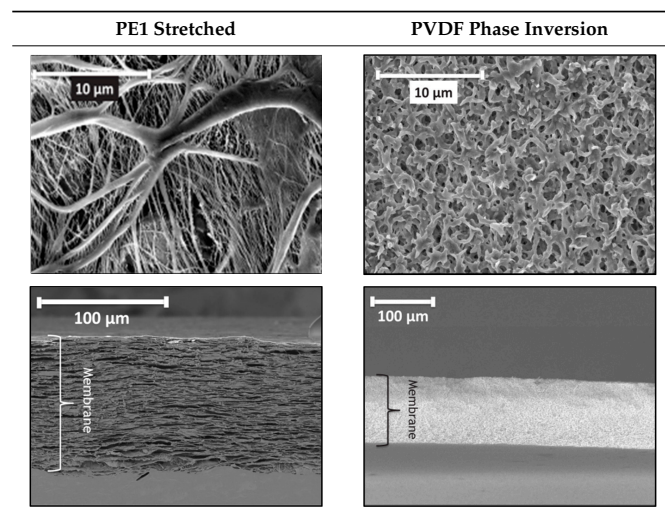
Table 2. Characteristics of the hydrophilic support membrane (polyethersulfone (PES)) and the membranes commonly used for membrane distillation (polyethylene (PE) and polyvinylidene fluoride (PVDF)).

Membrane	Θ (°)	d_{max} (μm)	d_{av} (μm)	Δ (μm)	E (%)	LEP (bar)
PES (Membrana, MicroPES)	26 ± 4	0.61 ± 0.04	0.56 ± 0.03	115 ± 1	75.2 ± 0.3	0
PE (Lydall, Solupor)	120 ± 1	0.32 ± 0.02	0.43 ± 0.02	99 ± 1	75.6 ± 0.6	3.9 ± 0.1
PVDF (Millipore, GVHP)	120 ± 3	0.44 ± 0.01	0.60 ± 0.01	119 ± 1	65.7 ± 0.9	2.3 ± 0.1

Table 3. Surface and cross-section images of the commercial polyethersulfone (PES) membrane and properties obtained using image analysis.

SEM	Surface 1	Surface 2	Cross-Section
Images			
Properties	$\epsilon_s = 22 \pm 4\%$ $d_{min,s} = 0.03 \pm 0.1 \mu\text{m}$ $d_{av,s} = 0.47 \pm 0.2 \mu\text{m}$ $d_{max,s} = 1.90 \pm 0.5 \mu\text{m}$ Pore density = 4.1 ± 0.7	$\epsilon_s = 8.8 \pm 0.5\%$ $d_{min,s} = 0.24 \pm 0.1 \mu\text{m}$ $d_{av,s} = 0.91 \pm 0.7 \mu\text{m}$ $d_{max,s} = 2.2 \pm 0.3 \mu\text{m}$ Pore density = 1.2 ± 0.2	$\delta = 113 \pm 1 \mu\text{m}$

The SEM images in Table 4 show a difference in membrane structure for the stretched PE membrane, which is more porous compared to the PVDF membrane. Both membranes have a symmetric cross-section. The PVDF membrane has a more open surface structure compared to the PES-membrane, while it has lower bulk porosity.

Table 4. SEM (Cold field emission scanning electron microscope) images of PE (polyethylene) and PVDF (polyvinylidene fluoride) commercial hydrophobic membrane.

3.2. Wetting Resistance of the Coating

Table 5 shows the water contact angle of the membranes coated in this study. The uncoated membrane has a hydrophilic water contact angle of 27° . After the application of the coatings, surface 1 is hydrophobic and has a water contact angle of at least 100° , confirming the hydrophobic character of the coatings. Without organic crosslinking agent (PFD solution only), the highest water contact angle of 117° for 5 wt. % solution (membrane 1) and 118° for a 10 wt. % solution (membrane 2) are achieved. This difference in water contact angle is statistically insignificant and therefore, the contact angle is considered to be independent of the concentration in the range from 5 and 10 wt. % for this system. When adding components with polymerizable functionalities to form the polymeric network, the fluorinated fraction decreases (membranes 3–5). This is visualized in a slightly reduced hydrophobicity on the coated surface compared to membrane 1 and 2, with a water contact angle ranging from 100° to 110° . For the Ak/T/D/BTFO2N system (3 and 4), the water contact angle is increased from 100° to 110° using a 5 and 30 wt. % solution respectively. The V/Mc/F13 system (5) achieves a water contact angle of 109° with a concentration of only 5 wt. % and including a polymeric network. The water contact angle of untreated surface 2 equals 28° after 0.5 s, whereas after the coating procedure the water contact angle after 0.5 s varies from 83° to 100° for membrane 1–4. For these membranes, the water contact angle continuously decreases over time. For membrane 1–3 the droplet disperses in the membrane only after 2 min. For membrane 4, the droplet sinks into the membrane within 2 min of contact time. For membrane 5, the uncoated side even shows a stable contact angle of 110° similar to the contact angle on the coated side. These observations show that the surface hydrophobicity on the uncoated side is also affected by the coating process, indicating that a part of the coating is able to pass through the entire membrane cross-section and is also applied (partially) on the uncoated side of the membrane. However, despite the increase in water contact angle, the membranes 1–4 are still wetted in membrane distillation and are considered as hydrophobic/hydrophilic membranes. Membrane 5 is considered as an entirely hydrophobic membrane. The measured liquid entry pressure for the different membranes varies from 1.6 to 3.5 bar, with a large variation for multiple measurements of the same membrane. This variation in liquid entry pressure is attributed to the inhomogeneity of the coatings, meaning that the coating is not applied equally on the entire membrane surface on some parts of the surface are not sufficiently hydrophobic. This becomes visible after submerging the membranes in water. While most regions are not wetted, some areas of the membrane surface are wetted, showing that the bar coater and the roll-to-roll system are not the preferred application methods when applying the coatings on porous membranes. The contact angles reported in Table 5 only consider the area of the membrane that was not wetted after submersion of the membrane in water. However, the inhomogeneous application of the coating with barcoater or the roll-to-roll system was also visible in the large spreading of the contact angle measurements of 20° when measuring at random spots on the membrane.

Table 5. Contact angle.

Membrane	Coating Components	Mass Fraction in Coating Solution	θ ($^\circ$)	
			Surface 1 (Coated Side)	Surface 2 (Uncoated Side)
Uncoated	-	-	27 ± 6 ¹	28 ± 4 ¹
1	PFD solution	5 wt. %	117 ± 1	$90 \pm 5 \rightarrow 62 \pm 5$ ²
2	PFD solution	10 wt. %	118 ± 1	$96 \pm 1 \rightarrow 73 \pm 6$ ²
3	Ak/T/D/BTFO2N	5 wt. %	100 ± 3	$100 \pm 1 \rightarrow 85 \pm 5$ ²
4	Ak/T/D/BTFO2N	30 wt. %	110 ± 1	83 ± 2 ¹
5	V/Mc/F13	5 wt. %	109 ± 1	110 ± 1

Legend: ¹ Droplet wets the membrane within 2 min; ² Contact angle after 0.5 s \rightarrow Contact angle after 2 min.

To improve the coating homogeneity, coating system 5 (V/Mc/F13, 5 wt. %) was selected for spray coating application. The single component systems (1 and 2) are not sufficiently stable (see Section 3.4), whereas the Ak/T/D/BTFO2N system (3 and 4) requires a higher amount of silica components to achieve the same contact angle (Table 5). This spray coating process ensures an improved homogeneity compared to the bar coater system. The coating was applied in two ways: (a) only on surface 1, resulting in a membrane with a hydrophobic and a hydrophilic side and (b) on both sides of the membrane, producing a membrane with two hydrophobic sides (Table 6). Membrane 6, coated on surface 1 only shows a slightly lower liquid entry pressure compared to membrane 7, coated on both sides.

Table 6. Contact angle and LEP of the coatings applied by the spray system.

Membrane	Coated Side	θ (°)		LEP (bar)
		Surface 1	Surface 2	
6	Surface side 1 only	97 ± 1	$41 \pm 3^*$	1.8 ± 0.2
7	Both sides	102 ± 1	107 ± 1	2.2 ± 0.1

* Droplet wets the membrane within 2 min.

3.3. Structure of the Coating

Apart from the contact angle measurements, another important issue is the possibility that the coating will block the pores. This reduces the porosity and pore size, and in the ultimate case, a dense membrane is obtained, obstructing the mass transport. Pore blockage can easily be seen by porometry because it reduces both the gas flow through the membrane and the pore size compared to the untreated membrane. For membranes 1–3 and 5–7, the pore sizes and the gas flows of the uncoated and coated membranes are equal. As an example, the pore size distribution obtained using porometry is presented for an untreated membrane and membrane 3 and 4 are given in Figure 7. For membrane 4, coated with a 30 wt. % solution, no pores are detected using porometry, indicating that the pores are completely blocked by the coating in this case. These measurements reveal that a 30% solution is not suitable for membrane modification since it significantly affects the porosity.

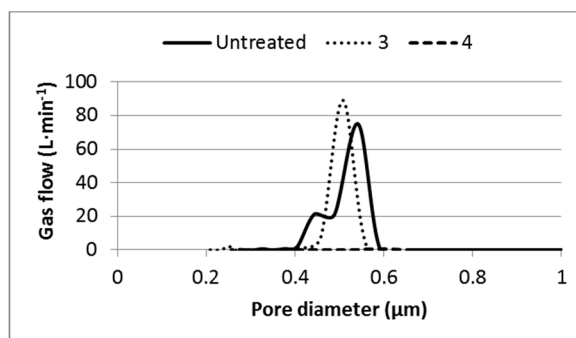


Figure 7. Pore size distribution untreated PES-membrane, membrane 3, and membrane 4 using porometry.

The position of the coating is investigated using energy-dispersive X-ray spectroscopy (EDX). As an example, Figure 8 shows the EDX spectrum of membrane 3. The peaks of the oxygen and sulfur atoms in the spectrum correlate with the presence of the PES membrane material or pores at the measured position. In the first 20 μm at surface 1, a first increase of the silicon and fluorine atoms is observed, which correlates with the position of the coating. A second increase is observed between 30 and 50 μm , which is also the densest zone of the membrane (Table 3) and therefore, more surface is

available to deposit the coating. In the part between 50 and 120 μm , the silicon and fluorine content is lower. The permeation of the coating might be inhibited by the denser structure of the membrane. Further in the membrane cross-section, the silicon and fluorine content decreases, but are not equal to zero. The increase of the oxygen and silicon at 120 to 140 μm is caused by the silicon glue used to fix the sample. Based on the EDX on the chemical composition, the structure is hydrophobic until a depth of at least 50 μm . Unfortunately, it is impossible to indicate the exact hydrophobicity or hydrophilicity in terms of a water contact angle at a certain point of the membrane cross-section based on the elemental composition obtained with EDX. Therefore, the exact hydrophobic thickness cannot be derived from these EDX figures.

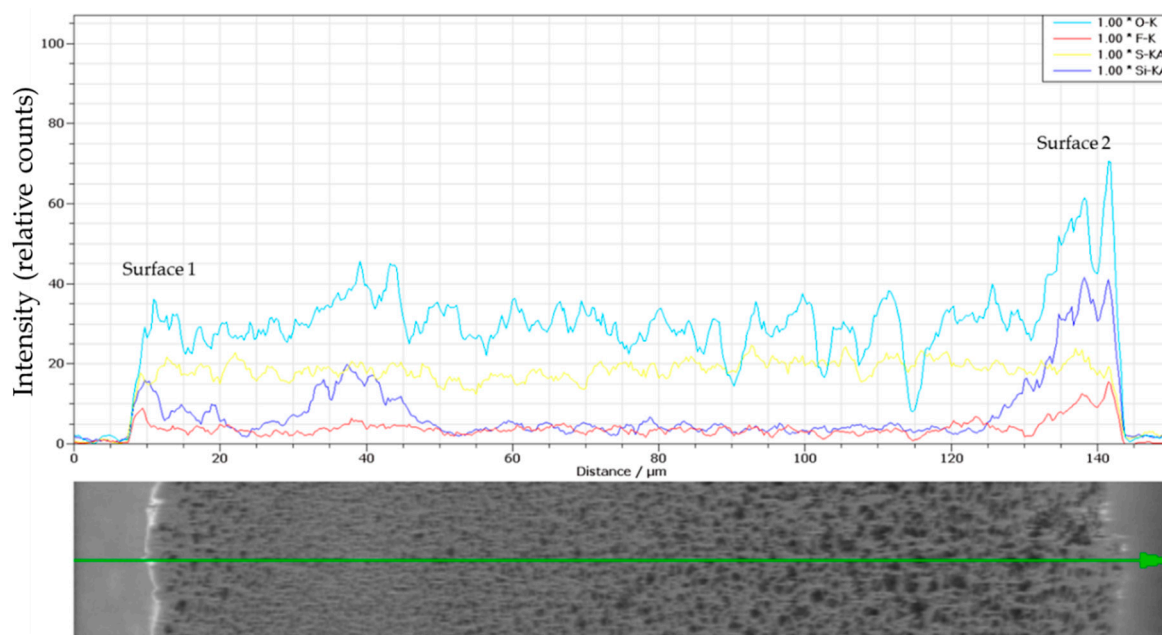


Figure 8. EDX (energy-dispersive X-ray spectroscopy) spectra of the cross section for membrane 3.

In summary, these results indicate that no difference in membrane structure in terms of thickness, pore size, and porosity was found for the coatings applied using less than 10 wt. % silanes in the coating solution. Only coating 4, with very high load of silanes, the MD-flux and N₂ flux during porometry decreased to zero, showed a strong difference, which is a strong indication for pore blocking.

3.4. Membrane Distillation Performance

The flux and energy efficiency of the membranes produced in this study are compared to the PVDF GVHP membrane from Millipore commonly used in the literature and to a PE membrane currently used in pilot scale membrane distillation modules (Table 2).

All coated membranes are coated on the same base membrane structure, except for membrane 4, where pore blocking occurs. The other membranes have equal porosity, pore size, and total thickness. However, the position of the coating and hence the thickness of the hydrophobic layer can be different. Since this thickness can affect the flux and energy efficiency of the membrane for desalination applications [20], a difference in MD performance is expected. Flux and energy efficiencies of the different membranes are summarized in Table 7.

Membranes 1 and 2 are single component systems without organic network formation and show immediate breakthrough of the salts. The membrane wetting is also visually observed after demounting the module. This indicates that the inorganic network formed by these coatings is not sufficient to provide stable coatings for the process conditions used in membrane distillation.

Membranes 3 and 4 use the same components, but with a difference in mass fraction of 5 wt. % and 30 wt. % respectively (Table 1). Membrane 3 shows a much higher flux of $16.2 \text{ kg}\cdot\text{m}^{-2}\cdot\text{h}^{-1}$ compared to membrane 4 with a flux of only $0.4 \text{ kg}\cdot\text{m}^{-2}\cdot\text{h}^{-1}$. This low flux of membrane 4 is caused by the pore blocking shown in Figure 7, which hinders the transport of water vapor through the membrane. This shows that a mass fraction of 5 wt. % silanes in the coating solutions is balancing between a sufficient hydrophobicity and avoiding obstruction of the pores, which occurred at concentrations of 30 wt. %.

The hydrophobic/hydrophilic membranes 3 and 6 show higher fluxes of about $16 \text{ kg}\cdot\text{m}^{-2}\cdot\text{h}^{-1}$ compared to membranes 5 and 7 with a flux of about $14 \text{ kg}\cdot\text{m}^{-2}\cdot\text{h}^{-1}$, which have two hydrophobic sides (Table 7). The effect of partial pore wetting on flux and heat transfer is comprehensively described in reference [47], where it was shown that an increase of the depth of pore wetting results in an increase of the flux. This difference in flux is explained by a different in hydrophobic non-wetted membrane thickness, which imposes the mass transport resistance for vapor transport. As discussed in the literature, the optimal hydrophobic thickness ranges from 10 to 60 μm using $35 \text{ g}\cdot\text{L}^{-1}$ NaCl [20,48–50]. While the membranes with two hydrophobic surfaces (5 and 7) are probably fully hydrophobic or at least they do not contain a wetted part, the cross-section of the hydrophobic/hydrophilic membrane structures (3 and 6) is partially wetted by the permeate liquid on surface side 2. Therefore, the hydrophobic layer thickness is much closer to the optimal values of 10–60 μm for the hydrophobic/hydrophilic membranes. The fluxes achieved are higher compared to the commercial PVDF membrane, whereas the commercial PE membrane shows a flux slightly higher compared to the membranes with two hydrophobic sides, but lower compared to the membranes with a hydrophobic/hydrophilic structure.

The energy efficiency varies from 43% to 55% and is lower compared to the commercial membranes and appears mainly to depend on the membrane base structure and porosity (Section 3.1). PE has the highest porosity and surface porosity and shows the highest energy efficiency as well. The energy efficiency of the PVDF membrane is negatively affected by the lower bulk porosity [14]. The coated PES membrane has relatively high bulk porosity, but as shown in Table 3, the membrane is not symmetric and has a more dense structure at the surface and in the first 100 μm . This causes less mass transport and more heat transport through the membrane in the first 60 μm , reducing the energy efficiency. Membranes applied with the same application systems (membrane 3 and 5 and membrane 6 and 7) have equal energy efficiency, regardless of the fact that the resulting membrane is a hydrophobic/hydrophilic membrane or a membrane with 2 hydrophobic surfaces. This can be explained by the independence of the energy efficiency as function of membrane thickness, which is shown by different authors [20,48]. This independency occurs because both heat transfer due to flux and heat transfer due to conduction are approximately inversely proportional to the membrane thickness. A high salt retention above 99.9% was measured for all membranes.

Table 7. Flux, energy efficiency and salt retention. Process conditions: $T_f = 60 \text{ }^\circ\text{C}$, $T_p = 45 \text{ }^\circ\text{C}$, $v = 0.13 \text{ m}\cdot\text{s}^{-1}$, NaCl concentration = $35 \text{ g}\cdot\text{L}^{-1}$.

Membrane	Structure	Flux ($\text{kg}\cdot\text{m}^{-2}\cdot\text{h}^{-1}$)	Energy Efficiency (%)	Salt Retention (%)
1	hydrophobic/hydrophilic	16.2 ± 0.5	Wetted	99.98 ± 0.01
2	hydrophobic/hydrophilic			
3	hydrophobic/hydrophilic	0.4 ± 0.3	-	99.99 ± 0.01
4	hydrophobic/hydrophilic	14.5 ± 0.5	50 ± 2	99.99 ± 0.01
5	2 hydrophobic surfaces	16.1 ± 0.1	44 ± 3	99.92 ± 0.06
6	hydrophobic/hydrophilic	13.9 ± 0.1	43 ± 5	99.99 ± 0.01
7	2 hydrophobic surfaces	12.0 ± 0.1	52 ± 2	99.99 ± 0.01
PVDF	hydrophobic	15.3 ± 0.4	67 ± 4	99.99 ± 0.01
PE	hydrophobic			

3.5. Medium Term Performance

The coating material applied on membranes 5–7 is advantageous for membrane distillation based on its superior wetting resistance and homogeneity. Membranes 5 and 6 were tested for a longer period. The flux and salt retention for membrane 6 are shown as an example in Figure 9, but similar results are obtained for membrane 5. The steady decrease in flux is caused by the increasing salt concentration, while jump in flux is explained by the addition of water to the feed solution after a certain amount of time to maintain the concentration at $35 \text{ g}\cdot\text{L}^{-1}$. During a period of 80 h, salt retention was always above 99.9% and flux remained constant. To confirm the stability of the coating on the active membrane surface, the LEP of the used membrane was measured. The initial LEP was 1.8, while the LEP of the membrane after 80 h of operation equals 1.4 bar. This reduction is caused by the reduced surface tension after long term exposure to salts, which is also reported in the literature [51]. However, this reduction is not severe enough to indicate that the coating is washed off during operation. In that case, 0.1 bar would already result in the penetration of liquid through the membrane.

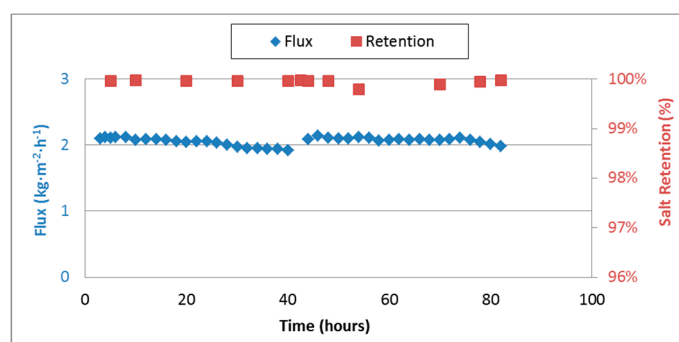


Figure 9. Long term experiment of membrane 6, $T_f = 45\text{ }^{\circ}\text{C}$, $T_p = 40\text{ }^{\circ}\text{C}$, $v = 0.13\text{ m}\cdot\text{s}^{-1}$, NaCl concentration = $35\text{ g}\cdot\text{L}^{-1}$.

4. Conclusions

Sol-gel coatings have proven their stability and excellent performance in many other applications and were successfully applied for the first time on a hydrophilic PES membrane with a suitable pore size, porosity, and thickness for application in membrane distillation. The sol-gel coatings provide sufficient hydrophobicity and resistance against membrane wetting, and the surface contact angle can be increased from 27° up to 110° . Based on this study, the V/Mc/F13 system was recommended because of its higher hydrophobicity at 5 wt. % loading of siloxanes. This allows for keeping the pores open for vapor transport. Moreover, it is possible to produce a membrane with two hydrophobic sides using the spraying technique on both sides of the membrane, whereas a membrane with a hydrophobic/hydrophilic structure is obtained when spraying the coating on only one side of the membrane. The membranes with a hydrophobic/hydrophilic structure are recommended for seawater desalination because the hydrophobic layer thickness is closer to the optimal thickness for flux. While the coated membranes achieve comparable fluxes, the energy efficiency is relatively low compared to the commercial membranes in the same conditions. The energy efficiency was found to be independent of the coating procedure, but is dependent on the base membrane structure. Therefore, further optimization of the base membrane structure is required to further improve the membrane performance of these types of membranes in membrane distillation.

Acknowledgments: L. Eykens thankfully acknowledge a Ph.D. scholarship provided by VITO.

Author Contributions: L.E. performed the membrane characterization and M.D. testing and wrote the paper. K.R. prepared the inorganic-organic coatings on the PES-substrate and corrected the manuscript. M.D., K.D.S., C.D., L.P. and B.V.D.B. guided the experiments, analysis and the writing process.

Conflicts of Interest: The authors declare no conflict of interest.

References

1. Zhang, P.; Knötig, P.; Gray, S.; Duke, M. Scale reduction and cleaning techniques during direct contact membrane distillation of seawater reverse osmosis brine. *Desalination* **2015**, *374*, 20–30. [[CrossRef](#)]
2. Kesieme, U.K. Mine Waste Water Treatment and Acid Recovery Using Membrane Distillation and Solvent Extraction. Ph.D. Thesis, Victoria University, Footscray, Australia, 2015.
3. Calabrò, V.; Drioli, E.; Matera, F. Membrane distillation in the textile wastewater treatment. *Desalination* **1991**, *83*, 209–224. [[CrossRef](#)]
4. Hickenbottom, K.L.; Cath, T.Y. Sustainable operation of membrane distillation for enhancement of mineral recovery from hypersaline solutions. *J. Membr. Sci.* **2014**, *454*, 426–435. [[CrossRef](#)]
5. Christensen, K.; Andresen, R.; Tandskov, I.; Norddahl, B.; du Preez, J.H. Using direct contact membrane distillation for whey protein concentration. *Desalination* **2006**, *200*, 523–525. [[CrossRef](#)]
6. Tomaszewska, M.; Gryta, M.; Morawski, A.W. Study on the concentration of acids by membrane distillation. *J. Membr. Sci.* **1995**, *102*, 113–122. [[CrossRef](#)]
7. Teoh, M.M.; Chung, T.S. Membrane distillation with hydrophobic macrovoid-free PVDF-PTFE hollow fiber membranes. *Sep. Purif. Technol.* **2009**, *66*, 229–236. [[CrossRef](#)]
8. Bonyadi, S.; Chung, T.S. Flux enhancement in membrane distillation by fabrication of dual layer hydrophilic-hydrophobic hollow fiber membranes. *J. Membr. Sci.* **2007**, *306*, 134–146. [[CrossRef](#)]
9. El-Bourawi, M.S.; Ding, Z.; Ma, R.; Khayet, M. A framework for better understanding membrane distillation separation process. *J. Membr. Sci.* **2006**, *285*, 4–29. [[CrossRef](#)]
10. Alkhudhiri, A.; Darwish, N.; Hilal, N. Membrane distillation: A comprehensive review. *Desalination* **2012**, *287*, 2–18. [[CrossRef](#)]
11. Lawson, K.W.; Lloyd, D.R. Membrane distillation. *J. Membr. Sci.* **1997**, *124*, 1–25. [[CrossRef](#)]
12. Schneider, K.; Hölz, W.; Wollbeck, R.; Ripperger, S. Membranes and modules for transmembrane distillation. *J. Membr. Sci.* **1988**, *39*, 25–42. [[CrossRef](#)]
13. Khayet, M.; Matsuura, T. *Membrane Distillation: Principles and Applications*; Elsevier B.V.: Amsterdam, The Netherlands, 2011.
14. Eykens, L.; De Sitter, K.; Dotremont, C.; Pinoy, L.; van der Bruggen, B. How to Optimize the Membrane Properties for Membrane Distillation: A Review. *Ind. Eng. Chem. Res.* **2016**, *55*, 9333–9343. [[CrossRef](#)]
15. Alklaibi, A.M.; Lior, N. Transport analysis of air-gap membrane distillation. *J. Membr. Sci.* **2005**, *255*, 239–253. [[CrossRef](#)]
16. Abu Al-Rub, F.A.; Banat, F.; Beni-Melhim, K. Parametric Sensitivity Analysis of Direct Contact Membrane Distillation. *Sep. Sci. Technol.* **2002**, *37*, 3245–3271. [[CrossRef](#)]
17. Jönsson, A.S.; Wimmerstedt, R.; Harrysson, A.C. Membrane distillation—A theoretical study of evaporation through microporous membranes. *Desalination* **1985**, *56*, 237–249. [[CrossRef](#)]
18. Ali, M.I.; Summers, E.K.; Arafat, H.A.; Lienhard, J.H.V. Effects of membrane properties on water production cost in small scale membrane distillation systems. *Desalination* **2012**, *306*, 60–71. [[CrossRef](#)]
19. Bahmanyar, A.; Asghari, M.; Khoobi, N. Numerical simulation and theoretical study on simultaneously effects of operating parameters in direct contact membrane distillation. *Chem. Eng. Process. Process Intensif.* **2012**, *61*, 42–50. [[CrossRef](#)]
20. Eykens, L.; Hitsov, I.; de Sitter, K.; Dotremont, C.; Pinoy, L.; Nopens, I.; van der Bruggen, B. Influence of membrane thickness and process conditions on direct contact membrane distillation at different salinities. *J. Membr. Sci.* **2016**, *498*, 353–364. [[CrossRef](#)]
21. Thomas, R.; Guillen-Burrieza, E.; Arafat, H.A. Pore structure control of PVDF membranes using a 2-stage coagulation bath phase inversion process for application in membrane distillation (MD). *J. Membr. Sci.* **2014**, *452*, 470–480. [[CrossRef](#)]
22. Song, Z.W.; Jiang, L.Y. Optimization of morphology and performance of PVDF hollow fiber for direct contact membrane distillation using experimental design. *Chem. Eng. Sci.* **2013**, *101*, 130–143. [[CrossRef](#)]
23. Tang, Y.; Li, N.; Liu, A.; Ding, S.; Yi, C.; Liu, H. Effect of spinning conditions on the structure and performance of hydrophobic PVDF hollow fiber membranes for membrane distillation. *Desalination* **2012**, *287*, 326–339. [[CrossRef](#)]

24. García-Payo, M.C.; Essalhi, M.; Khayet, M. Effects of PVDF-HFP concentration on membrane distillation performance and structural morphology of hollow fiber membranes. *J. Membr. Sci.* **2010**, *347*, 209–219. [[CrossRef](#)]
25. Kim, Y.; Rana, D.; Matsuura, T.; Chung, W.J. Influence of surface modifying macromolecules on the surface properties of poly(ether sulfone) ultra-filtration membranes. *J. Membr. Sci.* **2009**, *338*, 84–91. [[CrossRef](#)]
26. Essalhi, M.; Khayet, M. Surface segregation of fluorinated modifying macromolecule for hydrophobic/hydrophilic membrane preparation and application in air gap and direct contact membrane distillation. *J. Membr. Sci.* **2012**, *417–418*, 163–173. [[CrossRef](#)]
27. Khayet, M.; Matsuura, T. Application of surface modifying macromolecules for the preparation of membranes for membrane distillation. *Desalination* **2003**, *158*, 51–56. [[CrossRef](#)]
28. Tijjing, L.D.; Choi, J.S.; Lee, S.; Kim, S.H.; Shon, H.K. Recent progress of membrane distillation using electrospun nanofibrous membrane. *J. Membr. Sci.* **2014**, *453*, 435–462. [[CrossRef](#)]
29. Essalhi, M.; Khayet, M. Self-sustained webs of polyvinylidene fluoride electrospun nanofibers at different electrospinning times: 1. Desalination by direct contact membrane distillation. *J. Membr. Sci.* **2013**, *433*, 167–179. [[CrossRef](#)]
30. Tian, M.; Yin, Y.; Yang, C.; Zhao, B.; Song, J.; Liu, J.; Li, X.M.; He, T. CF₄ plasma modified highly interconnective porous polysulfone membranes for direct contact membrane distillation (DCMD). *Desalination* **2015**, *369*, 105–114. [[CrossRef](#)]
31. Wu, Y.; Kong, Y.; Lin, X.; Liu, W.; Xu, J. Surface-modified hydrophilic membranes in membrane distillation. *J. Membr. Sci.* **1992**, *72*, 189–196. [[CrossRef](#)]
32. Razmjou, A.; Arifin, E.; Dong, G.; Mansouri, J.; Chen, V. Superhydrophobic modification of TiO₂ nanocomposite PVDF membranes for applications in membrane distillation. *J. Membr. Sci.* **2012**, *415–416*, 850–863. [[CrossRef](#)]
33. Khemakhem, S.; Amar, R.B. Modification of Tunisian clay membrane surface by silane grafting: Application for desalination with Air Gap Membrane Distillation process. *Colloids Surf. A Physicochem. Eng. Asp.* **2011**, *387*, 79–85. [[CrossRef](#)]
34. Haas, K.-H.; Amberg-Schwab, S.; Rose, K. Functionalized coating materials based on inorganic-organic polymers. *Thin Solid Films* **1999**, *351*, 198–203. [[CrossRef](#)]
35. Kron, J.; Amberg-schwab, S.; Schottner, G. Functional coatings on glass using ORMOCER®-systems. Code: BP20. *J. Sol-Gel Sci. Technol.* **1994**, *2*, 189–192. [[CrossRef](#)]
36. Matějček, V.; Rose, K.; Hayer, M.; Pospíšilová, M.; Chomát, M. Development of organically modified polysiloxanes for coating optical fibers and their sensitivity to gases and solvents. *Sens. Actuators B Chem.* **1997**, *39*, 438–442. [[CrossRef](#)]
37. Liao, Y.; Wang, R.; Tian, M.; Qiu, C.; Fane, A.G. Fabrication of polyvinylidene fluoride (PVDF) nanofiber membranes by electro-spinning for direct contact membrane distillation. *J. Membr. Sci.* **2013**, *425–426*, 30–39. [[CrossRef](#)]
38. Khayet, M.; Khulbe, K.C.; Matsuura, T. Characterization of membranes for membrane distillation by atomic force microscopy and estimation of their water vapor transfer coefficients in vacuum membrane distillation process. *J. Membr. Sci.* **2004**, *238*, 199–211. [[CrossRef](#)]
39. Hou, D.; Dai, G.; Wang, J.; Fan, H.; Zhang, L.; Luan, Z. Preparation and characterization of PVDF/nonwoven fabric flat-sheet composite membranes for desalination through direct contact membrane distillation. *Sep. Purif. Technol.* **2012**, *101*, 1–10. [[CrossRef](#)]
40. Haas, K.H.; Amberg-Schwab, S.; Rose, K.; Schottner, G. Functionalized coatings based on inorganic-organic polymers (ORMOCER S) and their combination with vapor deposited inorganic thin films. *Surf. Coat. Technol.* **1999**, *111*, 72–79. [[CrossRef](#)]
41. Schottner, G.; Rose, K.; Posset, U. Scratch and Abrasion Resistant Coatings on Plastic Lenses—State of the Art, Current Developments and Perspectives. *J. Sol-Gel Sci. Technol.* **2003**, *27*, 71–79. [[CrossRef](#)]
42. Khayet, M.; Matsuura, T. Preparation and Characterization of Polyvinylidene Fluoride Membranes for Membrane Distillation. *Ind. Eng. Chem. Res.* **2001**, *40*, 5710–5718. [[CrossRef](#)]
43. Francis, L.; Ghaffour, N.; Alsaadi, A.S.; Nunes, S.P.; Amy, G.L. Performance evaluation of the DCMD desalination process under bench scale and large scale module operating conditions. *J. Membr. Sci.* **2014**, *455*, 103–112. [[CrossRef](#)]

44. Smolders, K.; Franken, A.C.M. Terminology for Membrane Distillation. *Desalination* **1989**, *72*, 249–262. [[CrossRef](#)]
45. Khayet, M. Solar desalination by membrane distillation: Dispersion in energy consumption analysis and water production costs (a review). *Desalination* **2013**, *308*, 89–101. [[CrossRef](#)]
46. Khare, V.P.; Greenberg, A.R.; Krantz, W.B. Vapor-induced phase separation—Effect of the humid air exposure step on membrane morphology: Part I. Insights from mathematical modeling. *J. Membr. Sci.* **2005**, *258*, 140–156. [[CrossRef](#)]
47. Gilron, J.; Ladizansky, Y.; Korin, E. Silica Fouling in Direct Contact Membrane Distillation. *Ind. Eng. Chem. Res.* **2013**, *52*, 10521–10529. [[CrossRef](#)]
48. Martínez, L.; Rodríguez-Maroto, J.M. Membrane thickness reduction effects on direct contact membrane distillation performance. *J. Membr. Sci.* **2008**, *312*, 143–156. [[CrossRef](#)]
49. Laganà, F.; Barbieri, G.; Drioli, E. Direct contact membrane distillation: Modelling and concentration experiments. *J. Membr. Sci.* **2000**, *166*, 1–11. [[CrossRef](#)]
50. Wu, H.Y.; Wang, R.; Field, R.W. Direct contact membrane distillation: An experimental and analytical investigation of the effect of membrane thickness upon transmembrane flux. *J. Membr. Sci.* **2014**, *470*, 2257–2265. [[CrossRef](#)]
51. Boubakri, A.; Bouguecha, S.A.-T.; Dhaouadi, I.; Hafiane, A. Effect of operating parameters on boron removal from seawater using membrane distillation process. *Desalination* **2015**, *373*, 86–93. [[CrossRef](#)]



© 2017 by the authors. Licensee MDPI, Basel, Switzerland. This article is an open access article distributed under the terms and conditions of the Creative Commons Attribution (CC BY) license (<http://creativecommons.org/licenses/by/4.0/>).